

Research Paper

The design of a hybrid parabolic solar dish–steam power plant: An experimental study

Ali Basem ^{a,*}, M. Moawed ^b, Mohammed H. Abbood ^c,
Wael M. El-Maghlany ^d

^a Air Conditioning Engineering Department, Faculty of Engineering, Warith Al-Anbiyaa University, Iraq

^b Mechanical Engineering Department, Faculty of Engineering at Shoubra, Benha University, Egypt

^c Mechanical Engineering Department, Faculty of Engineering, Kerbala University, Iraq

^d Mechanical Engineering Department, Faculty of Engineering, Alexandria University, Egypt



ARTICLE INFO

Article history:

Received 10 August 2021

Received in revised form 5 November 2021

Accepted 15 November 2021

Available online xxxx

Keywords:

Parabolic solar dish

Steam power plant

Experimental study

Thermodynamics model

Rankine cycle system

ABSTRACT

A unique and novel steam power station has been built using a concentrated solar dish, to generate electricity. The system was built based on recommendations by previous researchers about the possibility of obtaining high temperatures using a solar dish. The steam generated will be used to operate a mini steam station, after making some simple changes to fit the new working mechanism, while retaining the main working principles of large steam power stations. This was achieved by using the main elements found in a Rankine cycle system for steam power plant stations (turbine, generator, condenser and pump) and by adding auxiliary secondary components to facilitate its protection and operation all year round. A small station consisting of a solar dish (solar heater), works as a boiler connected to a turbine, this linked to an electric generator. Outlet working fluid travels to the condenser and is then recycled back to the solar heater by a pump. A prototype of the solar dish was built of diameter 3 m, an aperture area reaching 7.1 m², and focal length 1.41 m, covered with 2 mm glass/ silver mirrors. Data was gathered in situ in summer and winter, to test its performance under different weather conditions and changes in the amount of solar radiation, temperature and wind speed. The results show that the station was able to generate good quantities of energy, ranging from between 900–2000 W, working at 31%–34% overall efficiency. A statistical analysis of the system was also carried out using a SPSS software the results of high accuracy, the maximum value of the coefficient of determination (R^2), 85%–91.3%.

© 2021 The Author(s). Published by Elsevier Ltd. This is an open access article under the CC BY-NC-ND license (<http://creativecommons.org/licenses/by-nc-nd/4.0/>).

1. Introduction

Concentrating solar power (CSP), is a technology which works to increase the density of solar radiation. The outer surface of a solar dish is covered with curved glass mirrors, which direct solar radiation to a small point called the focus point. When heat energy has been concentrated and transferred to the focus point or absorber, this causes an increase in temperature, the absorber able to reach temperatures in excess of 250 °C. The solar dish, or so-called parabolic collector, is a modern technology that focuses a direct beam of solar radiation onto a single point, similar in action to an antenna that collects radio waves. The shape of the dish, which is parallel to the axis in the direction of the focus, reflects incoming solar radiation, regardless of where it falls

on the dish. Almost all the incident solar radiation is therefore reflected. One of the advantages of the solar dish is its high efficiency as it can reach 85% efficiency when used with a tracking system, the temperature generated in the receiver reaching up to 750 °C.

First records of the use of concentrating sunlight to a small point was by the scientist Archimedes (287–212 BC) (Aden and Meinel, 1977) when he focused solar rays which were used to burn Roman ships. This technique continued to be used in many applications until the construction of the first station in 1977 in Shenandoah, GA, of 1147m-diameter, parabolic solar dishes which produced 2.6 MW of power. Many researchers have since studied and developed the application of solar dishes to generate electricity (Abbas et al., 2011; Beltran et al., 2012; Wu et al., 2010; Nepveu et al., 2009; Zang et al., 2004), cooking (Balzar et al., 1996; Grupp et al., 2009; Badran et al., 2010), water heating (Mohammed, 2012; Dafle and Shinde, 2012) and water desalination and distillation (Srithar et al., 2016; El-Kassaby, 1991; Omara and Eltawil, 2013; Abubakkar et al., 2021). There has been much

* Corresponding author.

E-mail addresses: ali.basem@uowa.edu.iq (A. Basem),

mmoawed28@feng.bu.edu.eg (M. Moawed),

Mohammed.hassan@uokerbala.edu.iq (M.H. Abbood), elmaghlany@alexu.edu.eg

(W.M. El-Maghlany).

Nomenclature

$D_{con.}$	Concentrator Diameter, m
$D_{rec.}$	Receiver Diameter, m
S	Surface Area, m^2
$A_{Con.}$	Aperture Area of the Dish, m^2
$A_{rec.}$	Aperture Area of the Receiver, m^2
d	Depth of the Dish, m
f	Focal Length, m
C	Concentration ratio
Q_u	Useful Energy, W
$Q_{rec.}$	Energy on the Receiver Surface, W
Q_{loss}	Total Heat Loss, W
$Q_{rad.}$	Radiative Heat Loss, W
$Q_{conv.}$	Convective Heat Loss, W
$Q_{cond.}$	Conduction Heat Loss, W
Q_{It}	Total Heat Loss in the Turbine, W
Q_{lc}	Total Heat Loss in the Condenser, W
Q_{lp}	Total Heat Loss in the Pump, W
I_{Bn}	Direct Normal Irradiance, W/m^2
$T_{cav.}$	Cavity Temperature, $^{\circ}C$
T_{∞}	Ambient Temperature, $^{\circ}C$
$h_{conv,nat}$	Natural Convective, $W/m^2 K$
$h_{conv,forced}$	Forced Convective, $W/m^2 K$
$h_{ext.,cav.}$	External Surface of the Receiver, $W/m^2 K$
$K_{rec.}$	Thermal Conductivity of the Receiver, $W/m K$
k_{∞}	Thermal Conductivity of Air, $W/m K$
$k_{ins.}$	Thermal Conductivity of the Insulation $W/m K$
h_1	Specific Enthalpy Inlet to Solar Heater, KJ/Kg
h_2	Specific Enthalpy Inlet to Turbine, KJ/Kg
h_3	Specific Enthalpy Inlet to Condenser, KJ/Kg
h_4	Specific Enthalpy Inlet to Pump, KJ/Kg
Re	Reynolds Number
G_r	Grashof Number
V_w	Wind Speed, m/s
F_{sh}	Un-Shading Factor
\dot{m}	Mass Flow Rate, kg/s

Greek Symbols

Ψ	Rim Angle
θ	Acceptance Angle
θ_z	Solar Incidence Angle
β	Surface Tilt Angle
ρ_m	Concentrator Mirror Reflectance
Γ	Solar Interception Factor
α_{eff}	Effective Absorbance of the Receiver
σ	Steven–Boltzmann Constant
ε	Emissivity
γ	Receiver Tilt Angle

Subscripts

amb.	ambient
i	inlet
o	outlet
con.	concentrator
rec. or r.	receiver
abs.	absorber
ref.	reflector
cav.	cavity
CSP	Concentrating solar power
CFD	Computational Fluid Dynamic
ANN	Artificial neural network model
R^2	Coefficient of determination

aperture area and size of concentrator, focal length of the reflector concentrator, focal point diameter (receiver) and concentration ratio. These studies have focused on the development of the shape and design of the solar dish with a receiver. [Kongtragool and Wongwiset \(2005\)](#) presented a theoretical model to enhance performance and maximize the power of the solar dish/ Stirling system by calculating the optimal temperature of the conical receiver. [Ahmadi et al. \(2013a,b\)](#) developed a thermodynamic optimization model for a solar dish/ Stirling system which depended on the finite rate of heat transfer and regenerative heat loss of the engine. [Pavlovic et al. \(2021\)](#) used a parabolic solar dish as a cogeneration system to drive an organic Rankine cycle. A value of 48.96% energy efficiency was obtained, the payback period of the system established to be 6.28 years. [Kumar and Yadav \(2021\)](#) examined three different receiver diameters: 0.150 m, 0.228 m and 0.304 m. Maximum temperatures occurred in the 0.15 m diameter receiver, the receiver outer temperature dependent on solar intensity and wind speed. [Daabo et al. \(2016\)](#) examined three different geometries: cylindrical, conical and spherical, as the geometry of a cavity solar receiver is important when analyzing its optical and thermal behavior. They used the ray tracing method and Computational Fluid Dynamic (CFD) modeling, their results showing that a conical shaped receiver, absorbed a higher amount of reflected flux energy than other shapes. [Sardeshpande et al. \(2011\)](#) proposed a procedure to calculate the thermal performance of parabolic solar dishes used to generate steam. This study used the latent heat method to evaluate performance. They established the best possible performance of the system and discussed the possibility of using that procedure in concentrated solar energy systems. Other research ([Kaushika and Reddy, 2000](#); [Palavras and Bakos, 2006](#)) developed and measured the performance of a low - cost parabolic solar dish, proving that the solar dish concentrator is inexpensive compared to the performance and the applications it can be used in. Other researchers ([Kuang and Zhang, 2012](#); [Slavin et al., 2006](#); [Shanmugam and Christraj, 2005](#)) have been interested in studying the design and implementation of tracking systems to improve the tracking accuracy of dishes, thereby delivering maximum efficiency and producing more power.

The current study is focused on an original design, building a new, small steam power plant to generate electric power using parabolic solar dish. It is a completely new idea which means the solar dish can work directly with the Rankine cycle, replacing the steam boiler. Many modifications were carried out including replacing the boiler with a solar dish (solar heater) to generate enough thermal energy to convert water into superheated steam. The working mechanisms of the system will be explained here, the experimental results used to calculate the amount of electrical energy generated and the efficiency of the new system. More information is presented in [Fig. 1](#).

research ([Devlin, 2008](#); [Mohamed et al., 2012](#); [Mahmood and Al-Salih, 2018](#); [El Ouederni et al., 2009a](#); [Rafeeu and Ab Kadir, 2012](#); [Hafez et al., 2016](#)) on the design of the parameters of solar dish concentrator such as the material for the reflector, the

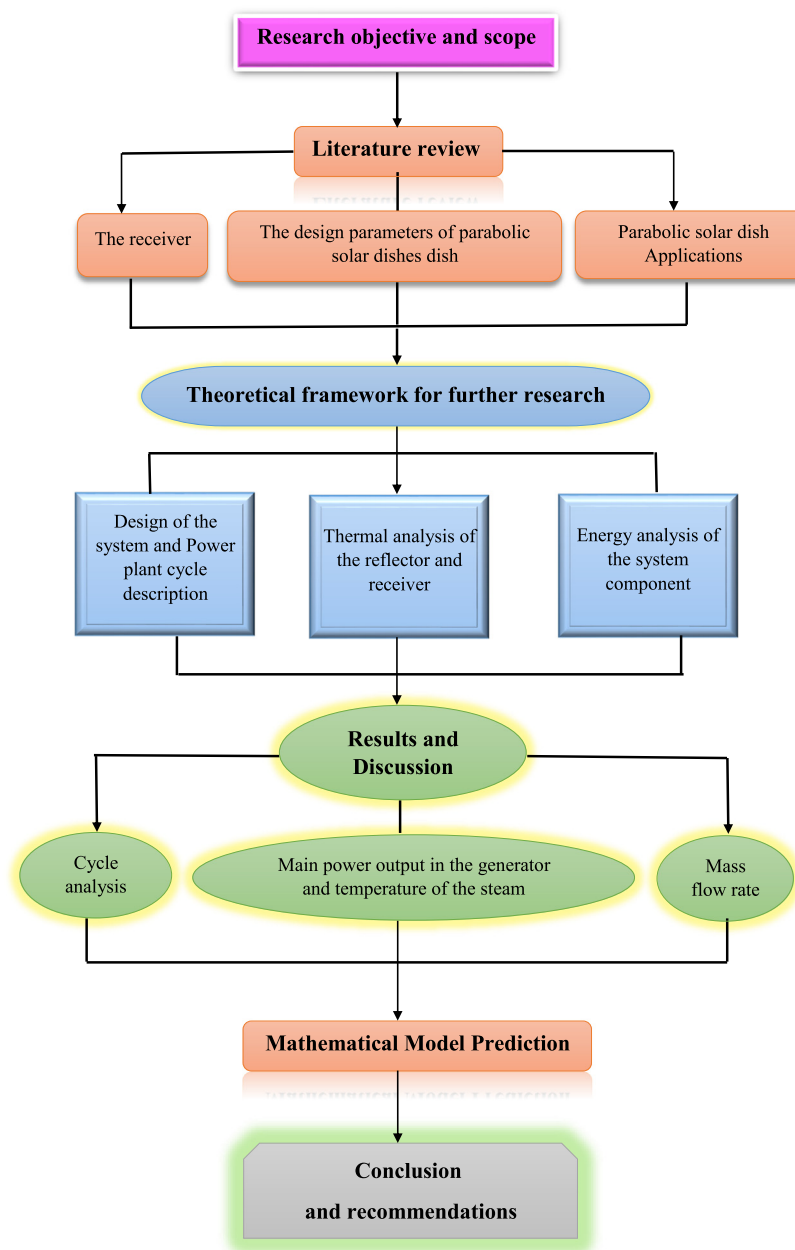


Fig. 1. Flowchart for present work.

2. Design of the system

The main components of the system are the solar heater, turbine, generator, condenser and pump. The auxiliary segment of the system is connected with the main components to control and identify the best working mechanisms, as shown in Fig. 2.

2.1. Solar heater (solar dish)

The main components of the solar heater are a parabolic solar dish connected to a two-axis tracking system. The solar dish is used instead of a boiler in the steam power plant, water entering after leaving the pump to generate steam which rotates the turbine. The solar dish is of 3 m diameter and is manufactured from steel covered with silver glass mirrors used as reflectors. Table 1 presents detailed information about the dish.

The frame of the solar dish was manufactured and built of galvanized rectangular steel and steel plates to house the glasses

mirrors. The external structure consists of three main components, the first a Galvanized rectangular steel circuit fixed to the ground to form a foundation for all the other elements to be fixed. This frame has to be strong enough to withstand many changes in weather, the most prominent the wind. This was achieved by using screws as previously indicated and seen in Fig. 3.

The second component is the upper segment that holds the dish. It stands on the circuit by means of a roller in order to provide smooth horizontal movement (east and west with the sun). with small motor with a belt which is have big moment and slow motion to provide this movement. This part is also made of galvanized rectangular steel. The third component is the dish, consisting of 17 pieces of curvilinear trapezoidal plate in the form of triangular plates that were assembled to form the circular shape of the collector dish. The dish itself was installed with the second component using ball bearings to provide vertical movement with a latitude angle (north and south with the sun)



Fig. 2. Parabolic solar dish–steam power plant system.

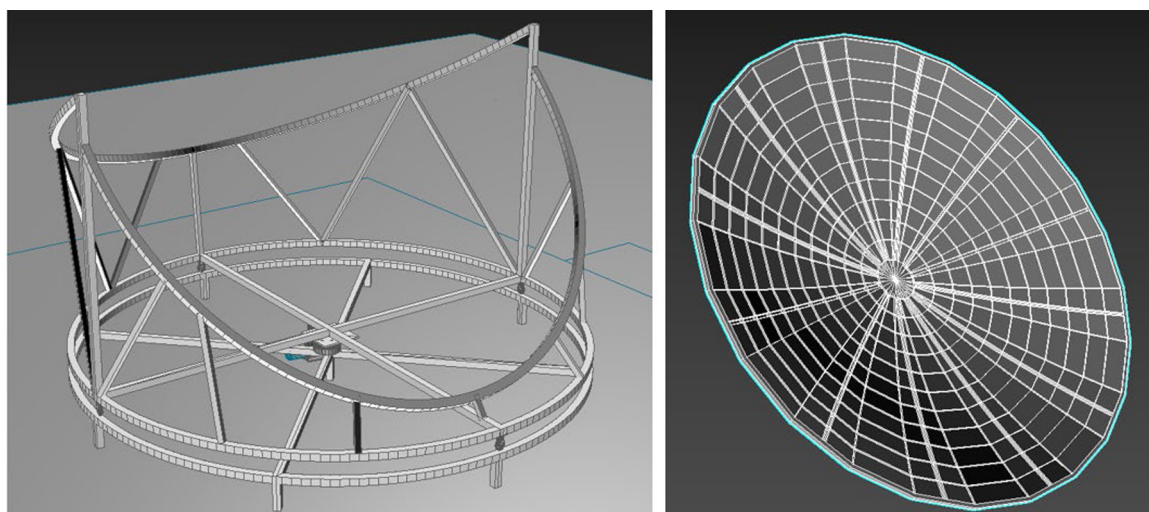


Fig. 3. The shape of the solar dish.

and to complete the dual axis tracking. The steel shafts are 2 mm thick, the steel plate 1 mm thick.

Glass/ silver mirrors are used as reflectors because of ready availability and low cost, fixed on the collector with silicon. It has a reflectivity of approximately 94% (Hafez et al., 2016), but is considered to be working at 90% in the current study. The mirrors were cut into small squares for easy installation and are 2 mm wide.

A two-axis, automatic tracking system was used in this design. Horizontal motion was achieved by using a motor with a belt and power supply connected to the converter. The vertical angle can be changed by hand through the ball bearings found between the dish and the structure it is mounted on.

The receiver

The receiver is the most important part of the solar parabolic dish as it connects incoming energy from the concentrator reflected by the parabolic dish, and the working fluid. As such, it needs to be efficient, minimizing heat loss and enhancing power output. Conical cavity stainless steel (Daabo et al., 2016; Kumar and Reddy, 2008; Loni et al., 2020; Harris and Lenz, 1985) plates at the focus point of the dish act as absorbers and as a boiler unit. Two layers of stainless-steel plates of 2 mm thickness, are used as heated layers, a 5 mm layer of foam (thermal conductivity 0.03 w/m. k (Calmidi and Mahajan, 1999)) between these acting as an insulation layer to minimize the heat loss from the wall, as shown in Fig. 4. Copper coil was used as an absorber inside the receiver because copper has a high thermal conductivity, reaching up to 401 w/m. k (Nath and Chopra, 1974)). The coil was 7 m

Table 1
Specification of the solar dish concentrator structure.

Parameters	Value	Units	Eq.	Ref.
Diameter of parabolic dish ($D_{con.}$)	3	m	-	-
Depth of concentrator dish (d)	0.4	m	$d = \frac{D_{con.}^2}{16f}$	Thakkar et al. (2015)
Focal length of dish (f)	1.41	m	$f = \frac{D_{con.}}{4 \tan(\frac{\psi_{rim}}{2})}$	Thakkar et al. (2015), Li and Dubowsky (2011)
Material of parabolic dish	Glass/ silver 2 mm	-	Reflectivity assumed 90%	Hafez et al. (2016), Harrison (2001)
Aperture area of dish ($A_{con.}$)	7.1	m ²	$A_{con.} = \frac{\pi}{4} D_{con.}^2$	Hafez et al. (2016), Thakkar et al. (2015)
The surface area (S)	11.52	m ²	$S = \frac{8\pi}{3} f^2 \left\{ \left[1 + \left(\frac{D_{con.}}{4f} \right)^2 \right]^{\frac{3}{2}} - 1 \right\}$	Gwani et al. (2015), El Ouederni et al. (2009b)
Rim angle of dish (ψ_{rim})	56	deg.	-	Sup et al. (2015), Nazemi and Boroushaki (2016)
Diameter of the receiver ($D_{rec.}$)	0.3	m	$D_{rec.} = \frac{f * \theta}{\cos \psi (1 + \cos \psi)}$	Thakkar et al. (2015)
Aperture area of receiver ($A_{rec.}$)	0.071	m ²	$A_{rec.} = \frac{\pi}{4} D_{rec.}^2$	Affandi et al. (2014), Reddy et al. (2013)
Geometric concentration ratio (C)	100	-	$C = \frac{A_{con.}}{A_{rec.}}$	El-Kassaby (1991), Fraser (2008)

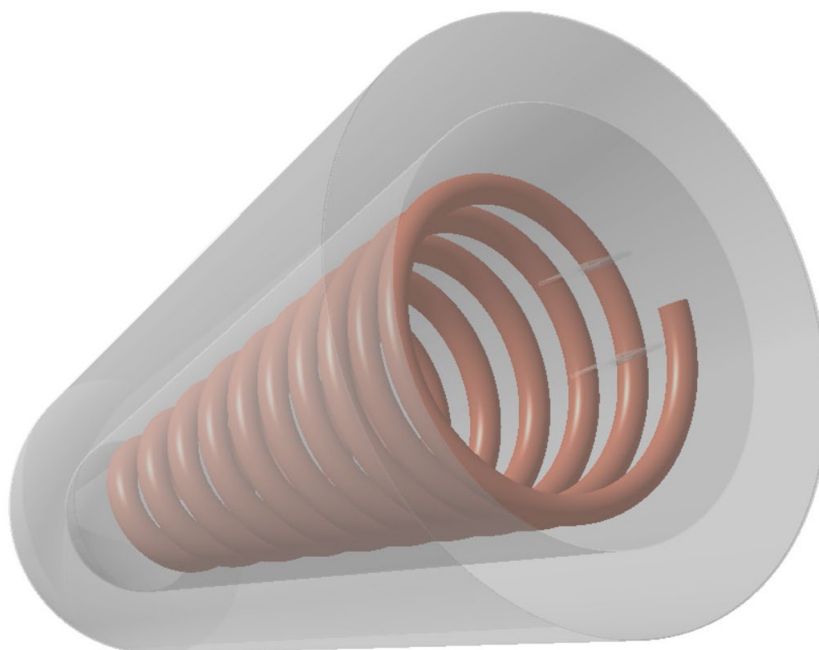


Fig. 4. Sketch of the receiver and copper coil.

long, 8 mm in diameter and 1 mm thick, forming a conical cavity receiver with a 30 cm bottom diameter tapering to 5 cm at the top.

2.2. The main system components and the properties of each, are presented in Table 2

There are secondary auxiliary components in the system to help gauge the workings and efficiency of the main working mechanism of the station. Details of these are given in Table 3 and Fig. 5.

• Power plant cycle description

The system starts working in the morning, the electric converter and battery operating the pump. The pump transfers the fluid to the solar dish to heat it, turning it into superheated steam which goes out to the turbine. Before entering the turbine, it passes through both the safety valve and the three-way valve

in order to establish whether it is within the temperature and pressure ranges required to enter the turbine. If it is not within the critical temperature and pressure range, it is returned to the solar dish until the required temperature and pressure is reached. As a result of the smaller amount of radiation available in the morning, the time the system starts working in the morning varies, as does the time when it closes down in the evening. This is further impacted by differences between summer and winter. Steam passes into the turbine to rotate the inlet blade and then rotate the electric generator. The fluid leaving the turbine passes to the condenser and the pump for recycling. There is also a valve in the system that controls the amount of flow after the pump to maintain the amount of flow. This allows changes dependent on season as in summer it will be between 0.75 – 1.25 L/sec because of the increased amount of solar radiation falling on the system. In winter, the amount of flow is fixed at 0.75 L/sec. due to a reduction in the amount of solar radiation.

Table 2
Components of the system.

Component	Type	Specification
Turbine	Impulse turbine single stage, twin nozzle	Inlet pressure 10 – 12 bar Back pressure 0.1 – 2 bar Inlet temperature 180 – 550 °C Turbine speed (rpm): 6600 – 8400 Output (rpm): 3000/ 3500 Maximum energy output about 4 kW Weight: 7.4 kg
Generator	Small electrical generator motor	Max. power output: 5 kW Rated power: 4.5 kW Rotation speed (rpm): 3000/ 3600 Rated voltage: 220 – 380 v Output power Type: AC Single Phase Frequency: 50 Hz Weight: 5 kg
Condenser	Mainly used in Refrigeration systems, dry cooling by air	Inlet pressure: 0.1 – 2 bar Inlet temperature: 110 – 80 °C Outlet temperature: 40 – 60 °C Structure: steel wires welded with Bundy tube Material: Bundy tube, steel wire, steel plates Bundy tube: diameter 6.3 mm and 0.7mm thickness Steel plate: wall thickness 0.5 mm
Pump	Water pump	Max. pressure Output: 16 bar Mass flow rate: 0.4 – 2 L/s Voltage: 24 VDC Power: 150 – 300 W Size: 140*65.5*89 mm

Table 3
Secondary auxiliary components.

Device	Type	Function
Three-way valve with temperature sensor	Three-way valve with sensor type PAKKENS	Prevents the fluid from passing through until the temperature and pressure required by the turbine is reached. Changes mass flow values with changes in solar irradiance.
Control valve (control mass flow rate)	Control valve 24 h (Timer controlled motorized ball valves)	
Safety valve	Works between 5-15 bar	Maintains the integrity of the system and prevents pressure increases above the permissible limit (10-12 bar)
Electrical converter with Battery	-	The converter is used with the battery to operate the pump in the morning and the motor that is used to rotate the solar dish in order to track the sun, to operate the control devices, and to provide the fan with power. It is also used to store some of the excess energy created during the day to provide power after sunset.
Tank	With 200 L capacity	Filled with water to make up, and compensate for, the small losses in the amount of water during work.
Manual valve	-	Used to open and closed the system by hand if there are any sudden changes that are not controllable.

3. The theoretical model

The theoretical model of the PDSC/ steam power plant station was used to calculate the useful heat energy gained by the working fluid in the receiver after evaluating the total heat losses from solar radiation after it has been concentrated from the reflector. This is followed by calculations of the amount of useful power generated in the turbine-generator to find the total efficiency of the PDSC and system components by using a first energy analysis to evaluate the thermal efficiency of the cycle.

3.1. Thermal analysis of the reflector and receiver

A thermodynamic model was used to measure the performance of the concentrator and receiver system by calculating output power and total efficiency, as shown in Fig. 6.

The useful energy in the receiver (Q_u) is defined as the energy gained by the working fluid and known as the difference between the energy reflected by the concentrator to the receiver ($Q_{rec.}$) and the total heat loss (Q_{loss}):

$$Q_u = Q_{rec.} - Q_{loss} \tag{1}$$



Fig. 5. Schematic diagram of the secondary auxiliary parts.

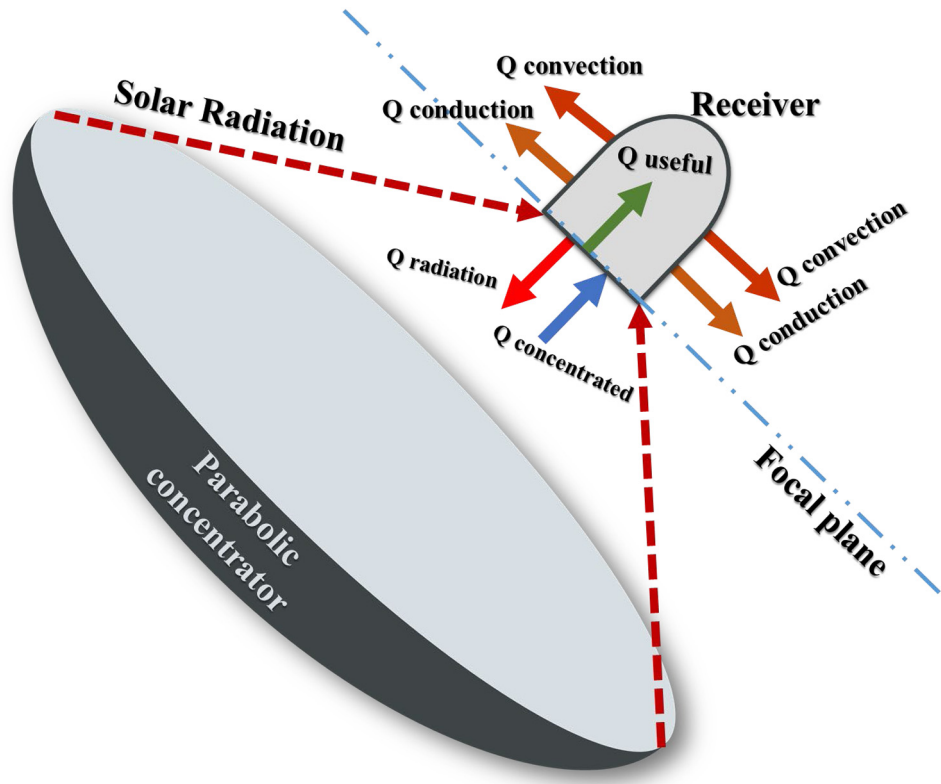


Fig. 6. Schematic diagram for the thermal analysis of the reflector and absorber.

- The energy reflected to the receiver is given by Eq. (2) (Li et al., 2011):

$$Q_{rec.} = \rho_m \Gamma I_{bn} A_{con}. \tag{2}$$

where ρ_m represents the concentrator mirror reflectance and Γ the solar interception factor. This was assumed to vary between 0.9 to 0.99 (Stine and Harrigan, 1985) so in this study, Γ was assumed to be 0.9 to allow for the possibility of maximum losses in the concentrator/receiver system to account for potential maximum losses. I_{bn} denotes direct intensity solar radiation incidence on the parabolic solar dish.

- Calculation of the total heat loss by the receiver was carried out by evaluating three types of loss in the receiver: conduction, convection and radiation.
- Radiative heat loss ($Q_{rad.}$) consists of two components: reflected and emitted radiation.

$$Q_{rad.} = Q_{rad.,ref.} + Q_{rad.,emi}. \tag{3}$$

Reflected radiation loss is given by Eq. (4) (Li et al., 2016):

$$Q_{rad.,ref.} = Q_{rec.}(1 - \alpha_{eff}) \tag{4}$$

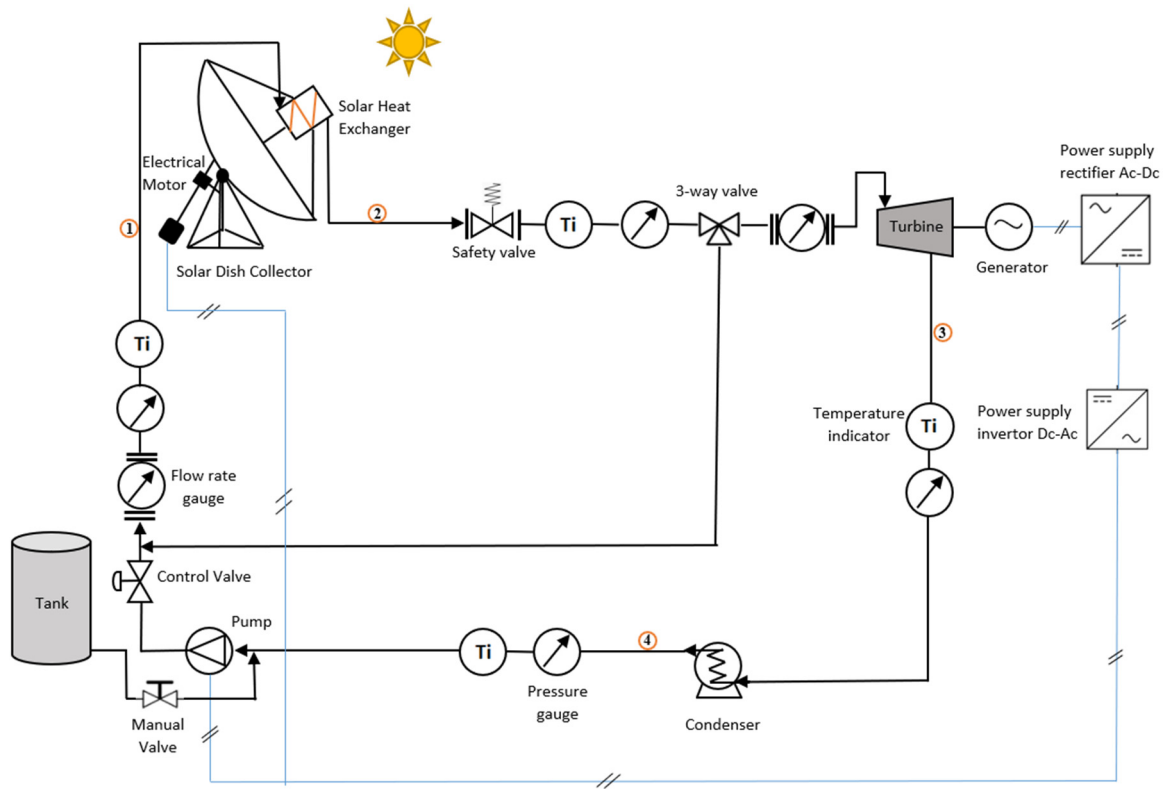


Fig. 7. Schematic diagram for the measurement devices and the mechanism of the system.

where α_{eff} is the effective absorbance of the receiver, the equation representing the absorptivity of the receiver material (Liao and Lin, 2015).

$$\alpha_{eff} = 1 - \frac{\alpha_{abs.,r}}{\alpha_{abs.,r} + (1 - \alpha_{abs.,r}) \frac{A_{rec.}}{A_{cav.}}} \quad (5)$$

The emitted radiation loss was calculated as (Chen and Chun, 2009):

$$Q_{rad,emi} = \sigma \epsilon_r A_{rec.} (T_{cav}^4 - T_{\infty}^4) \quad (6)$$

- Total convective loss (Q_{conv}) consists of two components: natural convection heat loss ($Q_{conv,nat}$) and forced convection heat loss ($Q_{conv,wind}$) (Zayed et al., 2020):

$$Q_{conv.} = (h_{conv.,nat.} + h_{conv.,forced}) A_{cav.} (T_{cav} - T_{\infty}) \quad (7)$$

Natural convective ($h_{conv.,nat}$) is effected by the size and diameter of the cavity and the absorber, the thermal conductivity of the absorber material, the tilt angle of the receiver and the temperature of the surroundings and cavity. It can be evaluated as (Castellanos et al., 2019):

$$h_{conv,nat} = \frac{K_{rec.}}{D_{rec.}} \left[0.088.Gr^{0.333} \cdot \left(\frac{T_{cav}}{T_{\infty}} \right)^{0.18} \cdot (\cos \gamma)^{2.47} \cdot \left(\frac{D_{rec.}}{D_{cav.}} \right)^{1.12-0.98 \left(\frac{D_{rec.}}{D_{cav.}} \right)} \right] \quad (8)$$

where γ is receiver tilt angle.

The forced convective ($h_{conv.,forced}$) depends on the receiver tilt angle (γ) and wind speed (V_w), as given by Ma (1993), Ma et al. (2019):

$$h_{conv,forced} = f(\gamma) \cdot v_w^{1.401} \quad (9)$$

where $f(\gamma)$ is defined as Ma et al. (2019):

$$f(\gamma) = 0.1634 + 0.7498 \sin \gamma - 0.5026 \sin^2 \gamma + 0.3278 \sin^3 \gamma \quad (10)$$

Caballero et al. (2017) recommend a receiver tilt angle (γ) of 75° .

- Conduction heat loss (Q_{cond}) is given as Zayed et al. (2019a,b)

$$Q_{cond} = \frac{(T_{cav} - T_{\infty})}{\frac{\ln \frac{D_{ro}}{D_{ri}}}{2\pi k_r L_r} + \frac{\ln \frac{D_{cav}}{D_{ro}}}{2\pi k_{ins} L_{ins}} + \frac{1}{h_{ext.,cav} A_{o,cav}}} \quad (11)$$

The external surfaces of the cavity and receiver ($h_{ext.,cav.}$) is given by Morgan (1975)

$$h_{ext.,cav.} = 0.148 Re^{0.633} \frac{k_{\infty}}{D_{cav.}} \quad (12)$$

3.2. Energy analysis of the system component

In order to apply energy analysis to the working fluid heat cycle of the parabolic dish solar concentrator/power plant, the system was provided with a set of measurement devices and sensors as shown in Fig. 7. These were fitted to find the required values for the design of the thermodynamics model for the system components. Conservation of mass and energy equations were applied to each component to calculate losses and efficiency.

Energy balance equations were applied to all components of the system to evaluate thermal efficiency for each component and for the cycle, as shown in Table 4 below:

4. Results and discussion

The purpose of this work was to produce electricity from solar energy and to consider the impact of different seasons on the operation of the system. Two sets of results were taken; one in

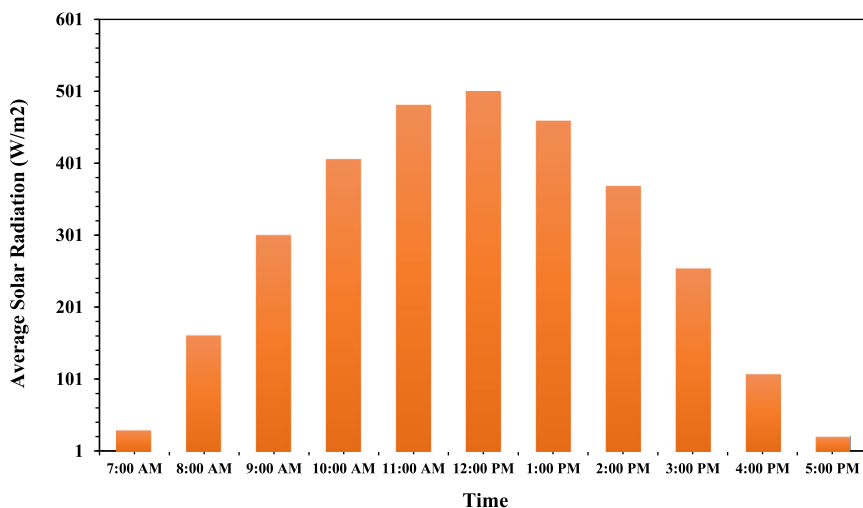


Fig. 8. Average total solar radiation through December in Iraq.

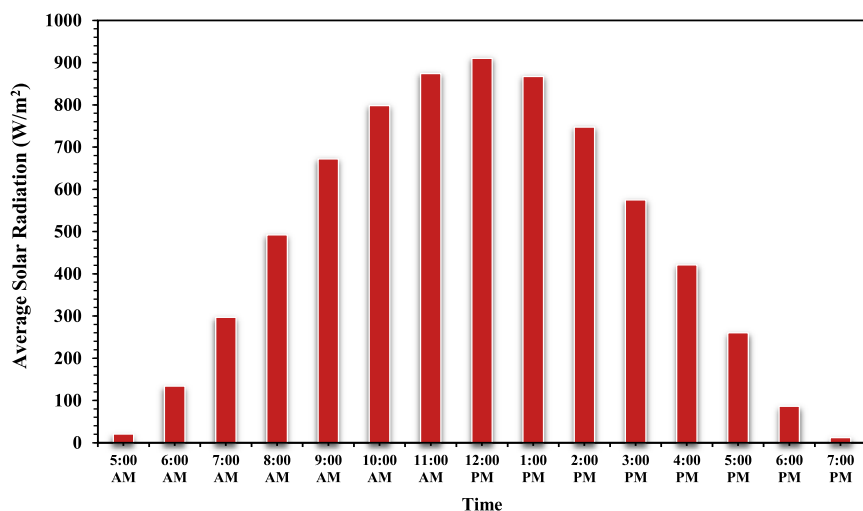


Fig. 9. Average solar radiation through June in Iraq.

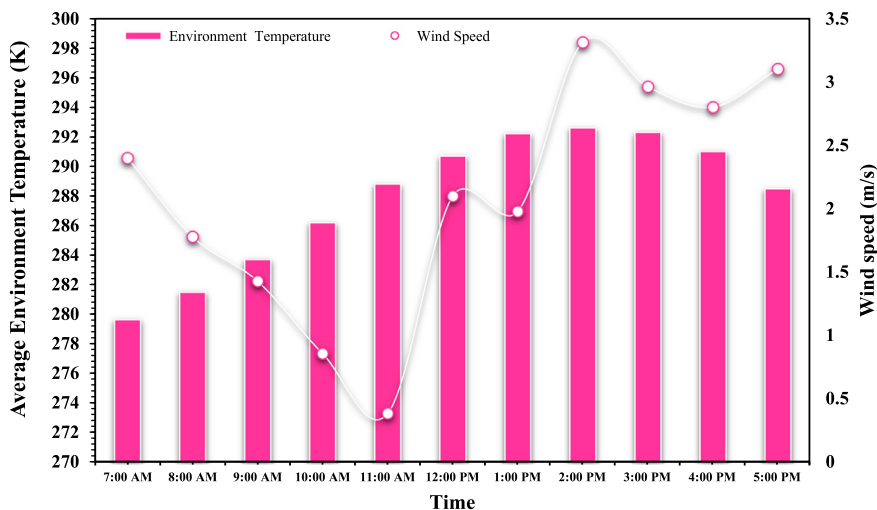


Fig. 10. Average environmental temperature and wind speed through December in Iraq.

each of December and June. In December, the mass flow rate was fixed at 0.75 L/sec at maximum solar radiation, this achieving 522 W/m², the turbine working at 10 bars between 180–450 °C.

In June, the solar radiation increased to above 800 W/m² (specifically reaching 908 W/m² in situ). This reading was taken on a specific day and is not seen throughout summer nor is it an

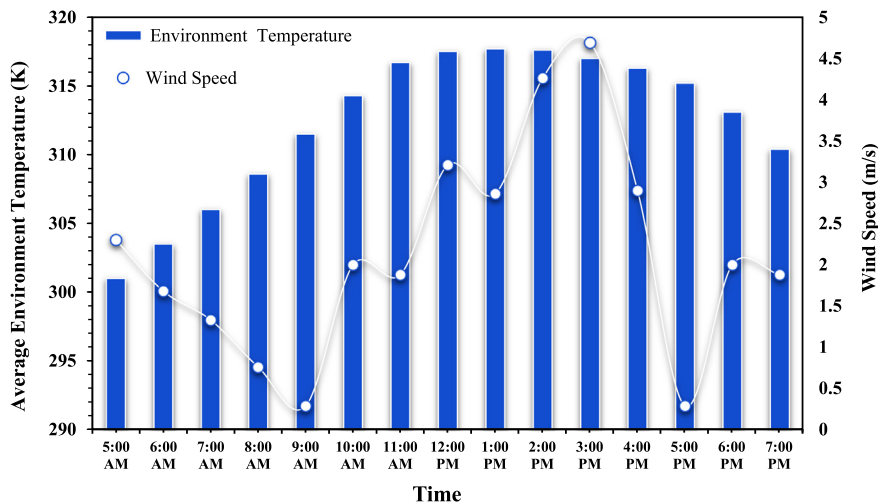


Fig. 11. Average environmental temperature and wind speed through June in Iraq.

Table 4

Energy equations and thermal efficiency equations for the system’s components.

Component	Energy Balance	Thermal efficiency
Solar heater	$Q_{in} = Q_{con.} - \sum Q_{loss} = \dot{m}_w(h_2 - h_1)$	$\eta_{th} = \frac{\dot{m}_w(h_2 - h_1)}{\text{total solar energy}}$
Turbine	$W_t = \dot{m}(h_2 - h_3) - Q_{it}$	$\eta_{th} = \frac{\dot{m}(h_2 - h_3)}{\dot{m}(h_2 - h_3) - Q_{it}}$
Condenser	$Q_{cond.} = \dot{m}(h_3 - h_4) - Q_{ic}$	$\eta_{th} = 1 - \frac{\dot{m}(h_3 - h_4) - Q_{ic}}{\dot{m}(h_3 - h_4)}$
Pump	$W_{pump} = \dot{m}(h_4 - h_1) + Q_p$	$\eta_{th} = \frac{\dot{m}(h_4 - h_1)}{\dot{m}(h_4 - h_1) + Q_p}$

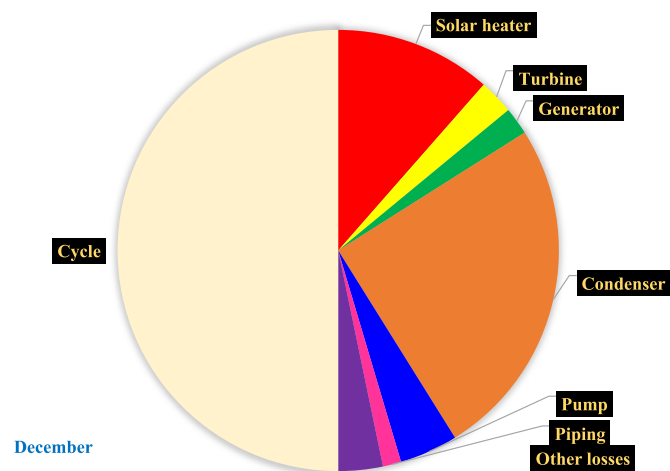


Fig. 12. Energy losses for each component and the power plant cycle.

average. Because of this difference, it was necessary to develop a way of dealing with the high quantity of solar radiation in summer in comparison to winter. This was achieved through the use of a control valve to change the mass flow rate as the solar radiation changed. The June results variable mass flow rate was fixed between 0.75 and 1.25 L/sec.

Figs. 8 and 9 present the average total beam solar radiation incidence in Iraq through December and June. Figs. 10 and 11 show the average temperature and wind speed through the same months.

Cycle analysis

The practical results obtained from the system, will be substituted in the energy balance of the components of the system to

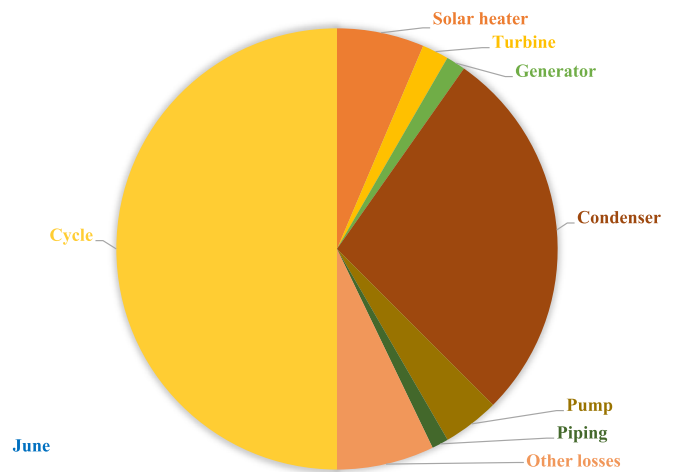


Fig. 13. Energy losses for each component and the power plant cycle.

evaluate the losses which occur in each component for the system cycle. The thermal efficiency for the system is also calculated as seen in Tables 5 and 6.

Other losses here represent the energy used by secondary auxiliary elements such as the motor used in the tracking system, the three-way valve and temperature sensor, the control valve for mass flow rate and the fan used with the condenser. These are calculated after evaluating the losses in each system, subtracting these from the amount of energy extracted from the receiver.

Table 5 shows that in December, the maximum thermal efficiency of the cycle is 32.7% at maximum solar radiation of 520 W/m², the maximum temperature reaching 400.1 °C. The total heat loss, energy efficiency and heat drop percentages, are given for each component. The condenser experiences 1090.58 W energy loss which represents 50.19% percent from the total energy loss in the system cycle, while the solar heater only has a 498.2 W energy loss, this 22.93% of the total energy lost from the cycle.

The system starts working at 10:00 am when the solar radiation is 380 W/m², shutting down at 3:00 pm at 399 W/m² solar radiation, because at a pressure of 10 bars, the minimum temperature required is 180 °C.

Table 6 presents the results for June when the maximum thermal efficiency of the cycle is 33.1% at a maximum solar radiation

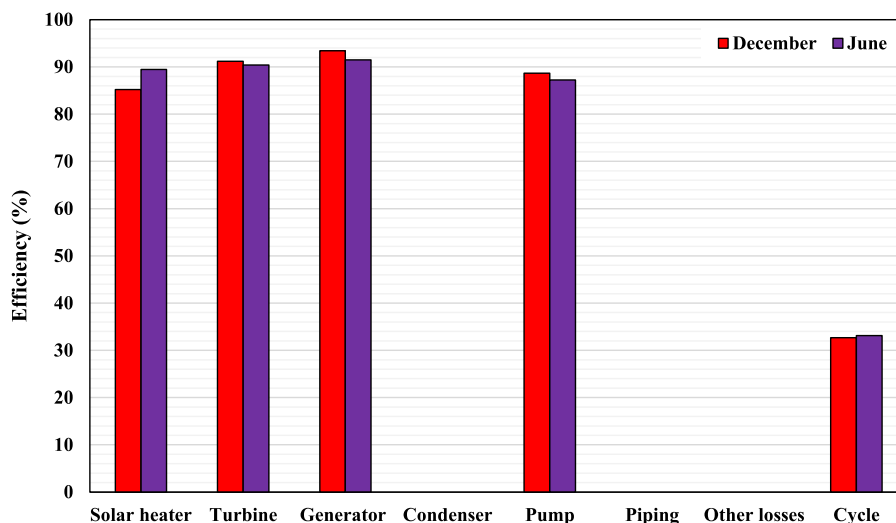


Fig. 14. Comparison of thermal efficiency between summer and winter for the main components and the power plant cycle.

Table 5

Energy balance of the components of the solar dish steam power plant and percentage ratios to total energy loss (December).

Element	Maximum losses Q_i (W)	Percent ratio	η_1
Solar heater	498.2	22.93	85.2
Turbine	110.9	5.1	91.2
Generator	87.23	4.14	93.4
Condenser	1090.58	50.19	–
Pump	186	8.56	88.65
Piping	58.4	2.69	–
Other losses	141.5	6.51	–
Cycle	2172.81	100	32.7

Table 6

Energy balance of the components of the solar dish steam power plant and percentage ratios to total energy loss (June).

Element	Maximum losses Q_i (W)	Percent ratio	η_1
Solar heater	466.54	12.77	89.45
Turbine	142.6	3.91	90.42
Generator	103.5	2.83	91.5
Condenser	2025	55.47	–
Pump	303	8.3	87.23
Piping	89.2	2.44	–
Other losses	521.1	14.27	–
Cycle	3650.94	100	33.1

of 908 W/m², the temperature reaching a high of 433.9 °C. In this table, the total heat losses in each component, energy efficiency and percentage of heat drop are given for each component. The condenser has an energy loss of 2025 W which represents 55.47% of the total energy loss in the system cycle, while the solar heater only experiences 466.54 W of energy loss, this 12.77% of the total energy lost from the cycle.

As shown above, there is a slight difference in values between the two tables. In June, the system comes on at 8:30am at 388 W/m² of solar radiation, switching off at 4:30pm at 377 W/m² solar radiation. It works for about 3 h longer than in winter and also gives out more power in comparison to winter because there is more solar radiation than in December, increasing the mass flow rate from 0.75 to 1.25 L/sec. The results from the turbine analysis show that energy loss in the turbine ranges between 90 and 142.6 W. Issues which can cause these energy losses include throttling–governing valves, heat loss from the body of the turbine, steam leakage from the glands of the turbine and internal irreversibility's.

As mentioned in the two tables above, energy losses vary across components. The thermal energy defined for each component and cycle in each table, are also different. Figs. 12 and 13 present the losses which occurred in each component and the total losses in the system cycle.

Fig. 14 presents a comparison of thermal efficiency between summer and winter, the results showing that the solar heater is more efficient in summer compared to winter. Likewise, when looking at the efficiency of the system in general, it is better in summer due to the increase in the number of working hours as mentioned above. As for the remaining components, efficiency is generally close across seasons, noting that it is higher in winter, because working conditions are more suitable in winter with relatively low environmental temperatures compared to summer.

• **Main power output in the generator and temperature of the steam**

Fig. 15 presents the relationship between the main power output and the steam inlet (to the turbine) temperature, for both summer and winter. There is an increase in the amount of electricity produced in summer as there is more solar radiation falling on the system compared to winter. The maximum power output in the generator in December reached 963 W with a steam temperature of 400.1 °C, while in June, the maximum power output in the generator was 1803.5 W with a steam temperature of 433.9 °C.

• **Mass flow rate**

Fig. 16 presents the mass flow rate where it can be seen that in winter, the mass flow rate is fixed at 0.75 L/s to keep the pressure and temperature entering the turbine in the range required to continue work and to protect it from damage against high temperatures or pressure.

Fig. 17 also presents the mass flow rate difference but for summer, where the flow rate changes according to changes in solar radiation. When the value of solar radiation reaches high levels, above 800 w/m², the mass flow rate will also change to keep the temperature and pressure within the range required, between 0.75–1.25 L/s.

5. Mathematical model prediction

5.1. Artificial neural network model (ANN)

An ANN model was developed using SPSS, to predict the power output (QG) from solar radiation, useful energy, heat loss, wind

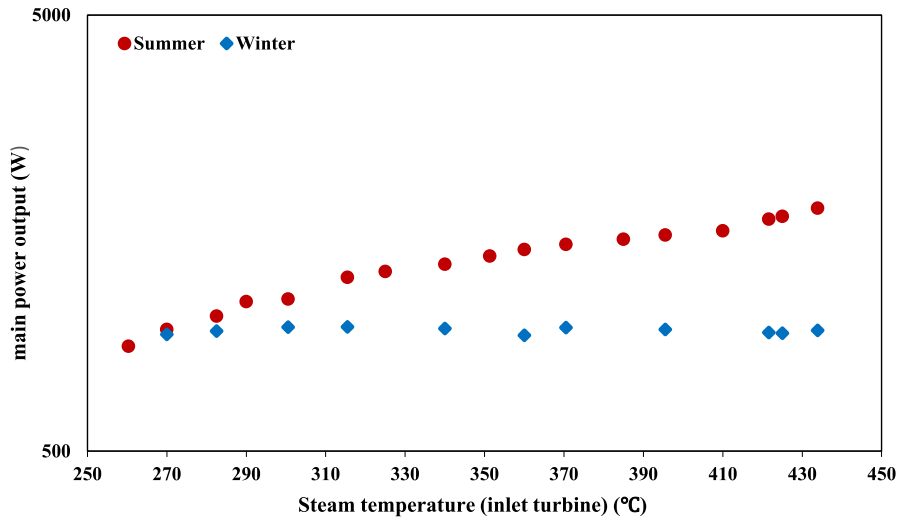


Fig. 15. Comparison of power output from the generator between summer and winter and steam temperature.

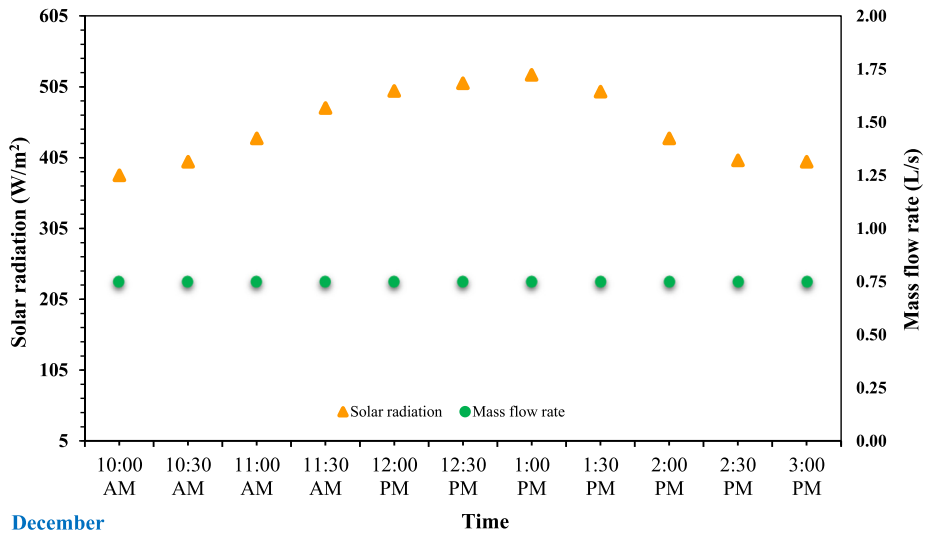


Fig. 16. Solar radiation with mass flow rate.

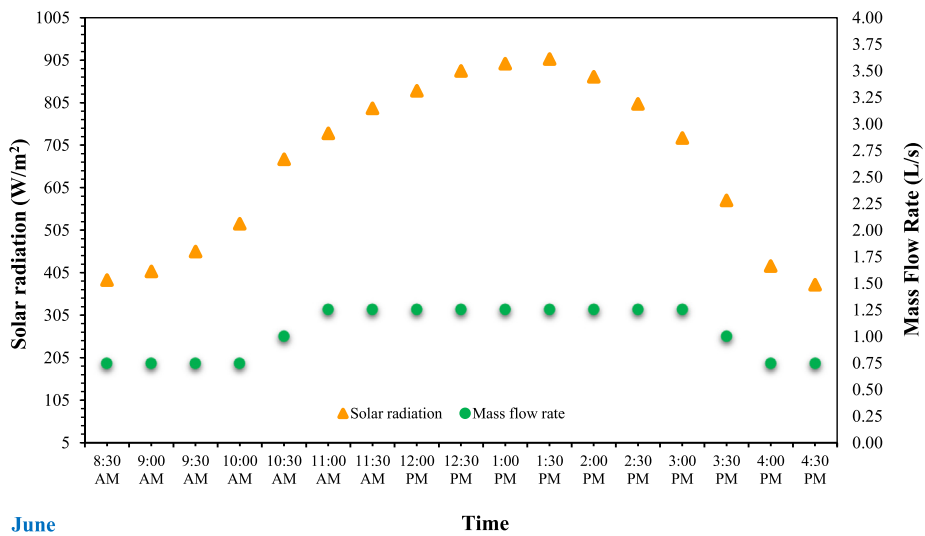


Fig. 17. Solar radiation with mass flow rate.

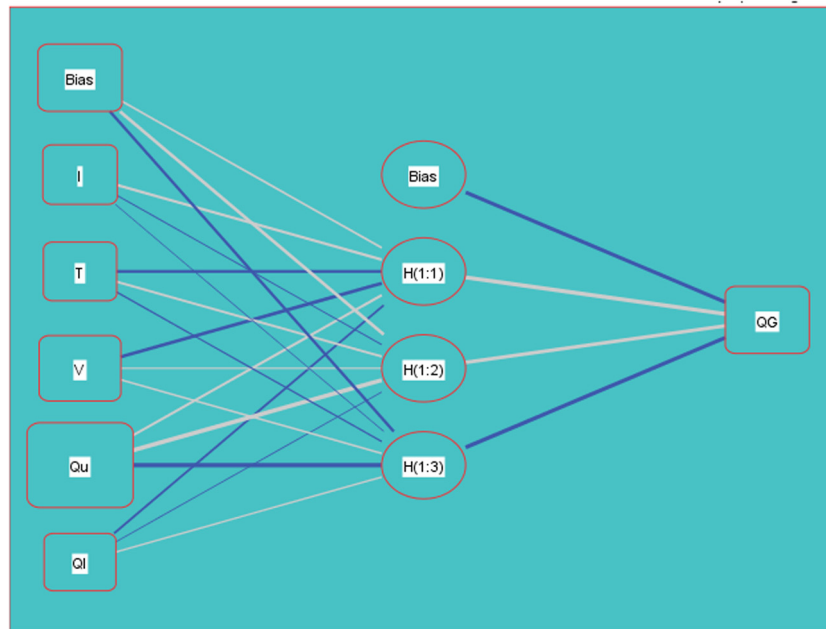


Fig. 18. ANN model architecture for December.

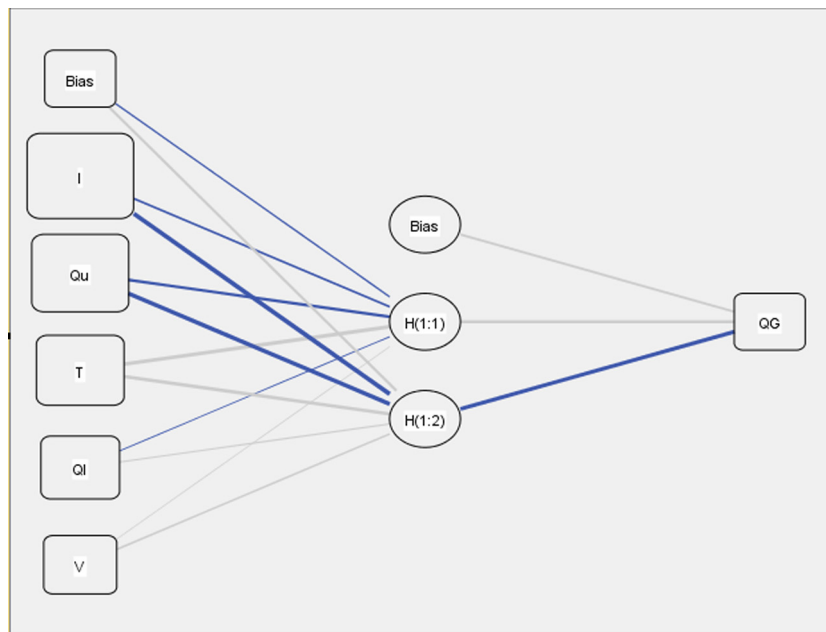


Fig. 19. ANN model architecture for June.

speed, and ambient temperature (I, Qu, Qi, V and T). In winter, the number of input data for the model is 61, this divided up to allow 42 for training, 10 for testing, and 8 for holdout. In summer, the number of input data for the model is 97, divided into 62 for training, 21 for testing and 14 for holdout. The rescaling method for data is standardization and the hidden layers are three of type hyperbolic tangent (Bekesiene et al., 2021). Figs. 18 and 19 show the resultant model architecture and the mathematical expression of the model which can be written as:

$$Q_G(winter) = -0.485 - 0.012I - 0.144T + 0.185V - 0.826Q_u + 0.168Q_i \tag{13}$$

$$Q_G(summer) = 0.861 - 1.903I + 1.041T + 0.76V - 1.706Q_u + 0.402Q_i \tag{14}$$

The predicted values vs observed values plot shows the module as having good levels of accuracy as shown in Figs. 20 and 21. For winter, the coefficient of determination R^2 is shown to be 92.5%, while in summer, this equals 0.85%. These percentages imply a good predictive capacity for these two models. According to these models, QG could be predicted under different operational conditions (Konishi, 2014).

To determine variations in the mode-predicted values for various independent variables, the importance of the independent variable is used. For December, it appears from Fig. 22, that the variable Qu (useful energy) has the greatest effect on how efficiently the solar system worked. Fig. 23 for June shows that solar radiation has the greatest effect on the system.

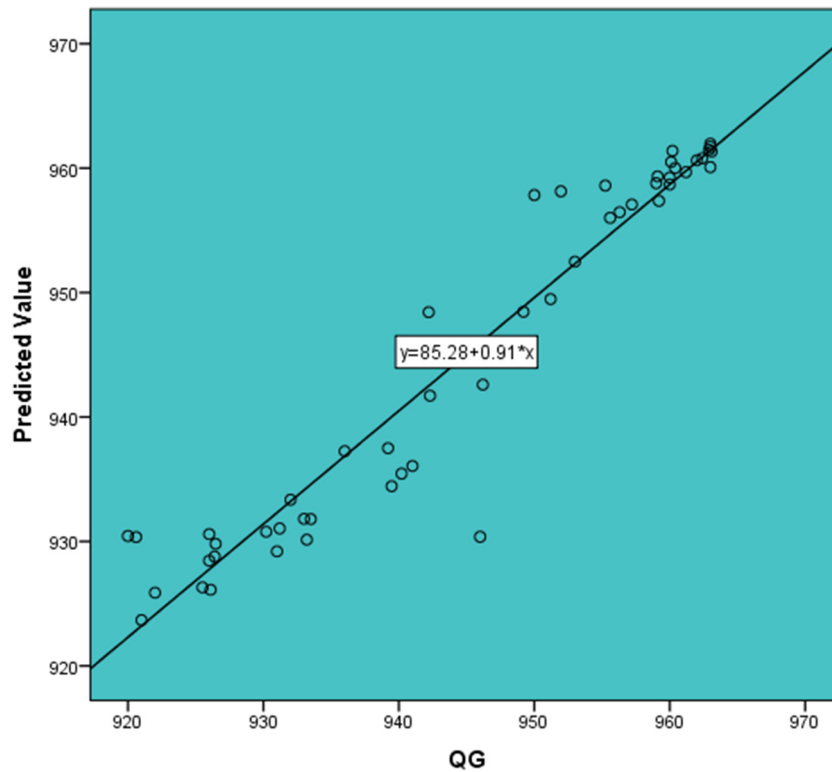


Fig. 20. The accuracy of the ANN model for December.

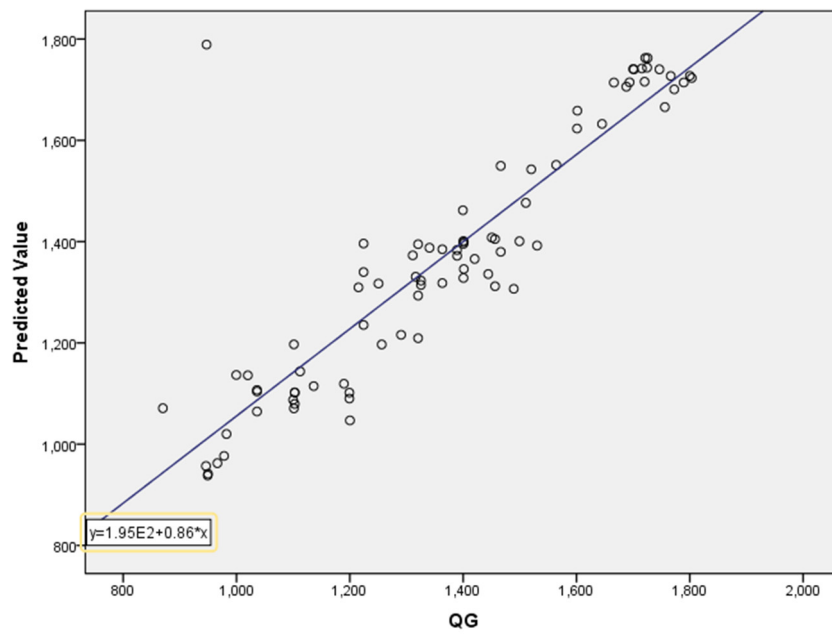


Fig. 21. The accuracy of the ANN model for June.

6. Conclusion

A new system was designed and built to generate electricity using a parabolic concentrated solar dish, modified by the addition of other components, making it similar to a steam power station. The solar dish was built according to the temperatures required and the amount of solar radiation expected to fall on the dish in both summer and winter. The output of power from the new system was good, this heralding the possibility of making

a combined steam power station to generate electricity using a concentrated solar dish. The work rate of the system was tested on different days, revealing a range of generated power falling between 900–2000 w, dependent on season. The performance of the proposed model was compared using the correlation coefficient (r). The suitability of the design of the structure of the neural network model was examined through trials, error, preparation and evaluation. The output prediction models of power are presented for December and June, the results showing that the Ann model

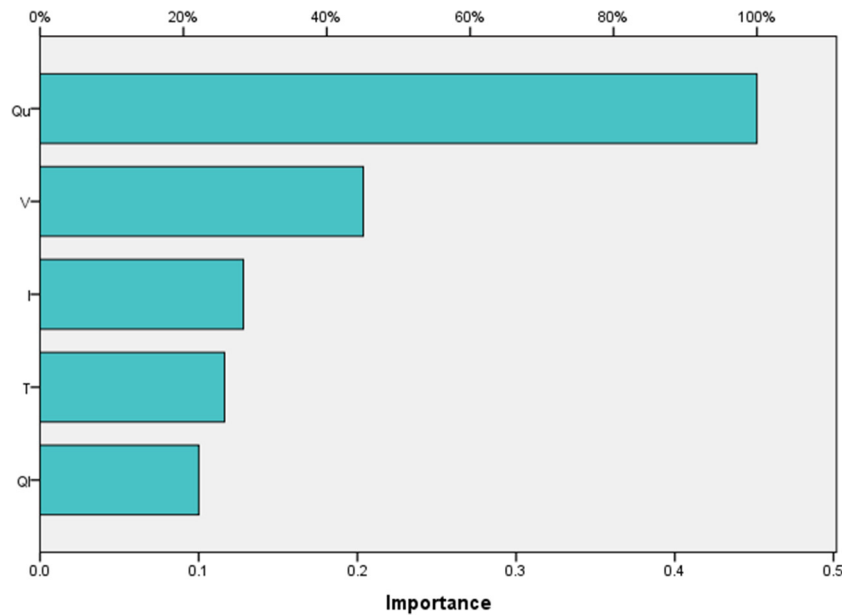


Fig. 22. Importance of the independent variables for the AI-Dora ANN model in December.

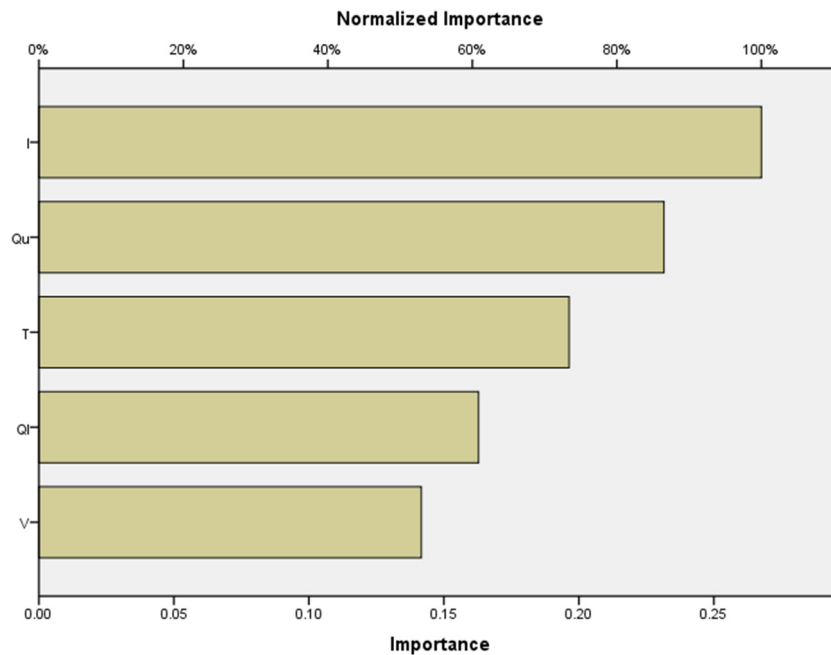


Fig. 23. Importance of the independent variables for the AI-Dora ANN model in June.

can estimate power output successfully. The results showed that useful energy from the solar heater have more effect on power output in December, while in June, solar radiation has more of an impact on power output in comparison to other parameters.

In summary:

- 1- Intensity of solar radiation: the maximum reading for solar radiation was 522 w/m² in December and 908 w/m² in June.
- 2- Mass flow rate: this was fixed at 0.75 L/sec in winter and varied between 0.75 – 1.25 L/sec in summer.
- 3- Maximum steam temperature: this was fixed between 180–550 °C, reaching 400.1 °C in December and 433.9 °C in June.

4- Losses: using energy equations for both seasons, the maximum cycle losses were 2172.81 w in December and 1766.66 w in June.

5- Efficiency: the cycle performed at 32.7% efficiency in December and 33.1% efficiency in June.

6- The main power output: in December, the maximum power output was 963 w and 1803.5 w in June.

7- The results are highly accurate as the maximum value of the coefficient of determination (R²) was 85% - 91.3%.

A large-scale parabolic solar dish concentrating-steam power plant is recommended as an effective alternative to a traditional large power plant.

CRedit authorship contribution statement

Ali Basem: Conception and design of study, Acquisition of data, Analysis and/or interpretation of data, Writing – original draft. **M. Moawed:** Conception and design of study, Writing – review & editing. **Mohammed H. Abbood:** Acquisition of data, Writing – review & editing. **Wael M. El-Maghlany:** Conception and design of study, Writing – review & editing.

Declaration of competing interest

The authors declare that they have no known competing financial interests or personal relationships that could have appeared to influence the work reported in this paper.

Acknowledgment

All authors approved the version of the manuscript to be published.

Appendix A. Supplementary data

Supplementary material related to this article can be found online at <https://doi.org/10.1016/j.ejgyr.2021.11.236>.

References

- Abbas, M., Boumeddane, N., Said, B., Chikouche, A., 2011. Dish stirling technology: A 100 MW solar power plant using hydrogen for Algeria. *Int. J. Hydrogen Energy* 36 (7), 4305–4314, <https://doi.org/10.1016/j.ijhydene.2010.12.114>.
- Abubakkar, A., Selvakumar, T., Rajagopal, P., Tamilvanan, A., 2021. Development of concentrating dish and solar still assembly for sea water desalination. *Mater. Today Proc.* 45, 974–980, <https://doi.org/10.1016/j.matpr.2020.03.043>.
- Aden, B. Meinel, Meinel, Marjorie P., 1977. *Applied Solar Energy: An Introduction*, Vol. 77. NASA STI/Recon Technical Report A, p. 33445, <https://agris.fao.org/agris-search/search.do?recordID=US201300543240>.
- Affandi, R., Gan, C.K., Ruddin, M., Ghani, A., 2014. Development of design parameters for the concentrator of parabolic dish (PD) based concentrating solar power (CSP) under Malaysia environment. *J. Appl. Sci. Agric.* 9 (11), 42–48, ISSN 1816-9112.
- Ahmadi, M.H., Mohammadi, S., Dehghani, M., Barranco-Jimenez, A.H., 2013a. Multi-objective thermodynamic-based optimization of output power of solar dish-stirling engine by implementing an evolutionary algorithm. *Energy Convers. Manage.* 75, 438–445, <https://doi.org/10.1016/j.enconman.2013.06.030>.
- Ahmadi, M.H., Sayyaadi, S., Dehghani, H., Hosseinzade, H., 2013b. Designing a solar powered stirling heat engine based on multiple criteria: maximized thermal efficiency and power. *Energy Convers. Manage.* 75, 282–291, <https://doi.org/10.1016/j.enconman.2013.06.025>.
- Badran, A.A., Yousef, N.K., Joudeh, R., Al Hamad, H., Halawa, K., Hassouneh, I.A., 2010. Portable solar cooker and water heater. *Energy Convers. Manage.* 51 (8), 1605–1609, <https://doi.org/10.1016/j.enconman.2009.09.038>.
- Balzar, A., Stumpf, S., Eckhoff, H., Ackermann, P., Grupp, M., 1996. A solar cooker using vacuum-tube collectors with integrated heat pipes. *Sol. Energy* 58 (1–3), 63–68, [https://doi.org/10.1016/0038-092X\(96\)00024-2](https://doi.org/10.1016/0038-092X(96)00024-2).
- Bekesiene, S., Smaliukiene, R., Vaicaitiene, R., 2021. Using artificial neural networks in predicting the level of stress among military conscripts. *Mathematics* 9 (6), 626, <https://www.mdpi.com/2227-7390/9/6/626>.
- Beltran, R., Velazquez, A.C., Espericueta, D., Saucedo, G., Perez, N., 2012. Mathematical model for the study and design of a solar dish collector with cavity receiver for its application in stirling engines. *J. Mech. Sci. Technol.* 26 (10), 3311–3321, <http://dx.doi.org/10.1007/s12206-012-0801-0>.
- Caballero, G.E.C., Mendoza, A.M., Martinez, E.E., Silva, V.R., Melian, O.J., Venturini, L.S., del Olmo, O.A., 2017. Optimization of a dish stirling system working with DIR-type receiver using multi-objective techniques. *Appl. Energy* 204, 271–286, <https://doi.org/10.1016/j.apenergy.2017.07.053>.
- Calmidi, V., Mahajan, R., 1999. The effective thermal conductivity of high porosity fibrous metal foams. *J. Heat Transfer*.
- Castellanos, L.S.M., Noguera, G.E.C., Caballero, A.L., De Souza, V.R.M., Cobas, E.E.S., Lora, A.L.G., Venturini, O.J., 2019. Experimental analysis and numerical validation of the solar dish/stirling system connected to the electric grid. *Renew. Energy* 135, 259–265, <https://doi.org/10.1016/j.renene.2018.11.095>.
- Chen, K., Chun, W., 2009. Radiation energy transfer and maximum conversion efficiency. *Appl. Energy* 86 (10), 2268–2271.
- Daabo, A.M., Mahmoud, S., Al-Dadah, R.K., 2016. The optical efficiency of three different geometries of a small scale cavity receiver for concentrated solar applications. *Appl. Energy* 179, 1081–1096, <https://doi.org/10.1016/j.apenergy.2016.07.064>.
- Dafle, V.R., Shinde, N.N., 2012. Design, development & performance evaluation of concentrating monoaxial scheffler technology for water heating and low temperature industrial steam application. *Int. J. Eng. Res. Appl.* 2 (6), 1179–1186.
- Devlin, M.R., 2008. Investigation of an alpha-parabolic solar concentrator dish. El-Kassaby, M.M., 1991. New solar cooker for parabolic square dish: Design and simulation. *Renew. Energy* 1 (1), 59–65, [https://doi.org/10.1016/0960-1481\(91\)90104-W](https://doi.org/10.1016/0960-1481(91)90104-W).
- El Ouederni, A.R., Salah, M.B., Askri, F., Nasrallah, M.B., Aloui, F., 2009a. Experimental study of a parabolic solar concentrator. *Rev. Energ. Renouvelables* 12 (3), 395–404, <https://revue.cder.dz/index.php/rer/article/view/149>.
- El Ouederni, A., Salah, F., Askri, M.B., Nasrallah, M.B., Aloui, F., 2009b. Experimental study of a parabolic solar concentrator. *J. Renew. Energies* 12 (3), 395–404, <https://revue.cder.dz/index.php/rer/article/view/149>.
- Fraser, P.R., 2008. *Stirling Dish System Performance Prediction Model*. University of Wisconsin-Madison.
- Grupp, M., Balmer, B., Beall, H., Bergler, J., Cieslok, D., Hancock, M., Schröder, G., 2009. On-line recording of solar cooker use rate by a novel metering device: prototype description and experimental verification of output data. *Sol. Energy* 83 (2), 276–279, <https://doi.org/10.1016/j.solener.2008.08.0025>.
- Gwani, M., Abubakar, G.A., Abbas, M., Allah, M.N., Danyaro, J., 2015. Design, fabrication and experimental study of solar parabolic dish concentrator for remote area application. *Int. J. Sci. Basic Appl. Res. (IJSBAR)* 23 (1), 230–241.
- Hafez, A., Soliman, K., El-Metwally, M., Ismail, A., 2016. Solar parabolic dish stirling engine system design, simulation, and thermal analysis. *Energy Convers. Manage.* 126, 60–75, <https://doi.org/10.1016/j.enconman.2016.07.067>.
- Harris, J.A., Lenz, T.G., 1985. Thermal performance of solar concentrator/cavity receiver systems. *Sol. Energy* 34 (2), 135–142, [https://doi.org/10.1016/0038-092X\(85\)90170-7](https://doi.org/10.1016/0038-092X(85)90170-7), <https://www.sciencedirect.com/science/journal/0038092X>.
- Harrison, J., 2001. Investigation of Reflective Materials for the Solar Cooker, Vol. 24. Florida Solar Energy Center.
- Kaushika, N., Reddy, K., 2000. Performance of a low cost solar paraboloidal dish steam generating system. *Energy Convers. Manage.* 41 (7), 713–726, [https://doi.org/10.1016/S0196-8904\(99\)00133-8](https://doi.org/10.1016/S0196-8904(99)00133-8), <https://www.researchgate.net/journal/Energy-Conversion-and-Management-0196-8904>.
- Kongtragool, B., Wongwises, S., 2005. Optimum absorber temperature of a once-reflecting full conical concentrator of a low temperature differential Stirling engine. *Renew. Energy* 30 (11), 1671–1687, <https://doi.org/10.1016/j.renene.2005.01.003>.
- Konishi, S., 2014. *Introduction to Multivariate Analysis: Linear and Nonlinear Modeling*. CRC Press, <https://doi.org/10.1201/b17077>.
- Kuang, J., Zhang, W., 2012. Design and implementation of tracking system for dish solar thermal energy based on embedded system. In: *Knowledge Discovery and Data Mining*. Springer, pp. 31–38.
- Kumar, N.S., Reddy, K., 2008. Comparison of receivers for solar dish collector system. *Energy Convers. Manage.* 49 (4), 812–819, <https://doi.org/10.1016/j.enconman.2007.07.026>, <https://www.researchgate.net/journal/Energy-Conversion-and-Management-0196-8904>.
- Kumar, V., Yadav, A., 2021. Experimental investigation of parabolic dish concentrator with various sizes of receiver. *Mater. Today Proc.* 44, 4966–4971, <https://doi.org/10.1016/j.matpr.2020.12.883>.
- Li, L., Dubowsky, S., 2011. A new design approach for solar concentrating parabolic dish based on optimized flexible petals. *Mech. Mach. Theory* 46 (10), 1536–1548, <https://doi.org/10.1016/j.mechmachtheory.2011.04.012>, <https://www.researchgate.net/journal/Mechanism-and-Machine-Theory-0094-114X>.
- Li, Z., Tang, J., Du, D., Li, T., 2011. Study on the radiation flux and temperature distributions of the concentrator-receiver system in a solar dish/stirling power facility. *Appl. Therm. Eng.* 31 (10), 1780–1789, <https://doi.org/10.1016/j.applthermaleng.2011.02.023>, <https://www.sciencedirect.com/science/journal/13594311>.
- Li, S., Xu, X., Luo, Y., Quan, G., Ge, Y., 2016. Optical performance of a solar dish concentrator/receiver system: Influence of geometrical and surface properties of cavity receiver. *Energy* 113, 95–107, <https://doi.org/10.1016/j.energy.2016.06.143>, <https://www.sciencedirect.com/science/journal/03605442>.
- Liao, T., Lin, J., 2015. Optimum performance characteristics of a solar-driven stirling heat engine system. *Energy Convers. Manage.* 97, 20–25, <https://doi.org/10.1016/j.enconman.2015.03.027>.
- Loni, R., Asli-Areh, B., Ghobadian, A., Kasaean, S., Gorjian, G., Najafi, E.A., Bellos, E., 2020. Research and review study of solar dish concentrators with different nanofluids and different shapes of cavity receiver: Experimental tests. *Renew. Energy* 145, 783–804, <https://doi.org/10.1016/j.renene.2019.06.056>, <https://www.sciencedirect.com/science/journal/09601481>.
- Ma, R.Y., 1993. *Wind Effects on Convective Heat Loss from a Cavity Receiver for a Parabolic Concentrating Solar Collector*. Sandia National Labs, Albuquerque, NM (United States), California State.

- Ma, L., Li, J., Wang, S., Li, J., Zhao, W., Li, M.E., Zayed, Q., Shao, M., Sun, Y., Buildings, 2019. A thermal-dissipation correction method for in-situ soil thermal response test: Experiment and simulation under multi-operation conditions. *Energy Build.* 194, 218–231, <https://doi.org/10.1016/j.enbuild.2019.04.014>.
- Mahmood, Y.H., Al-Salih, R.Y., 2018. Experimental study of two different types of solar dish characteristics and its efficiency based on Tikrit, Iraq weather conditions. *J. Phys. Conf. Ser.* <https://iopscience.iop.org/article/10.1088/1742-6596/1032/1/012006/meta>.
- Mohamed, F.M., Jassim, Y.h., Mahmood, A.S., 2012. Design and study of two axis tracking system. *Tikrit J. Pure Sci.* 17 (4), <https://www.iasj.net/iasj/article/72071>, <https://www.iasj.net/iasj/journal/199/issues>.
- Mohammed, Ladan Ibrahim, 2012. Design and development of a parabolic dish solar water heater. *Int. J. Eng. Res. Appl.* 2 (1), 822–830.
- Morgan, V.T., 1975. The overall convective heat transfer from smooth circular cylinders. In: *Adv. Heat Transfer*. Elsevier, pp. 199–264, [https://doi.org/10.1016/S0065-2717\(08\)70075-3](https://doi.org/10.1016/S0065-2717(08)70075-3).
- Nath, P., Chopra, K., 1974. Thermal conductivity of copper films. *Thin Solid Films* 20 (1), 53–62, [https://doi.org/10.1016/0040-6090\(74\)90033-9](https://doi.org/10.1016/0040-6090(74)90033-9), <https://www.sciencedirect.com/science/journal/00406090>.
- Nazemi, S.D., Boroushaki, M.J., 2016. Design, analysis and optimization of a solar dish/stirling system. *Int. J. Renew. Energy Dev.* 5 (1), <http://dx.doi.org/10.14710/ijred.5.1.33-42>.
- Nepveu, F., Ferriere, A., Bataille, F., 2009. Thermal model of a dish/Stirling systems. *Sol. Energy* 83 (1), 81–89, <https://doi.org/10.1016/j.solener.2008.07.008>.
- Omara, Z., Eltawil, M.A., 2013. Hybrid of solar dish concentrator, new boiler and simple solar collector for brackish water desalination. *Desalination* 326, 62–68, <https://doi.org/10.1016/j.desal.2013.07.019>.
- Palavras, I., Bakos, G., 2006. Development of a low-cost dish solar concentrator and its application in zeolite desorption. *Renew. Energy* 31 (15), 2422–2431, <https://doi.org/10.1016/j.renene.2005.11.007>, <https://ideas.repec.org/s/eee/renene.html>.
- Pavlovic, S., Bellos, Z., Said, E., 2021. Cogeneration system driven by solar dish concentrators. *Environ. Prog. Sustain. Energy* e13644.
- Rafeeu, Y., Ab Kadir, M.Z.A., 2012. Thermal performance of parabolic concentrators under Malaysian environment: A case study. *Renew. Sustain. Energy Rev.* 16 (6), 3826–3835, <https://doi.org/10.1016/j.rser.2012.03.041>.
- Reddy, V. Siva, Kaushik, S., Tyagi, S., 2013. Exergetic analysis and performance evaluation of parabolic dish stirling engine solar power plant. *Int. J. Energy Res.* 37 (11), 1287–1301, <https://doi.org/10.1002/er.2926>, <https://www.researchgate.net/journal/International-Journal-of-Energy-Research-1099-114X>.
- Sardeshpande, V.R., Chandak, A.G., Pillai, I.R., 2011. Procedure for thermal performance evaluation of steam generating point-focus solar concentrators. *Sol. Energy* 85 (7), 1390–1398, <https://doi.org/10.1016/j.solener.2011.03.018> <https://www.researchgate.net/journal/Solar-Energy-0038-092X>.
- Shanmugam, S., Christraj, W., 2005. The tracking of the sun for solar paraboloidal dish concentrators. *J. Sol. Energy Eng.* 127 (1), 156–160, <https://doi.org/10.1115/1.1824103>.
- Slavin, V., Bakos, T., Milovidova, G., Finnikov, K., 2006. Space power installation based on solar radiation collector and MHD generator. *IEEE Trans. Energy Convers.* 21 (2), 491–503, <https://doi.org/10.1109/TEC.2005.860401>.
- Srithar, K., Rajaseenivasan, N., Karthik, M., Periyannan, T., Gowtham, M., 2016. Stand alone triple basin solar desalination system with cover cooling and parabolic dish concentrator. *Renew. Energy* 90, 157–165, <https://doi.org/10.1016/j.renene.2015.12.063>.
- Stine, W.B., Harrigan, R.W., 1985. *Solar energy fundamentals and design*.
- Sup, B.A., Zainudin, T.Z.S., Ali, R.A., Bakar, M.F., Ming, G.L., 2015. Effect of rim angle to the flux distribution diameter in solar parabolic dish collector. *Energy Procedia* 68, 45–52, <https://doi.org/10.1016/j.egypro.2015.03.231>, <https://www.sciencedirect.com/science/journal/18766102>.
- Thakkar, V., Doshi, A., Rana, A., 2015. Performance analysis methodology for parabolic dish solar concentrators for process heating using thermic fluid. *J. Mech. Civ. Eng.* 12 (1), 101–114.
- Wu, S.-Y., Xiao, L., Li, Y.R., 2010. A parabolic dish/AMTEC solar thermal power system and its performance evaluation. *Appl. Energy* 87 (2), 452–462, <https://doi.org/10.1016/j.apenergy.2009.08.041>.
- Zang, C., Li, X., Li, F., Zheng, B., Li, A., 2004. Structural design and analysis of the dish solar thermal power system. In: *2nd International Energy Conversion Engineering Conference*. <https://doi.org/10.2514/6.2004-5645>.
- Zayed, M., Zhao, Y., Du, A., Kabeel, J., Shalaby, S., 2019a. Factors affecting the thermal performance of the flat plate solar collector using nanofluids: A review. *Sol. Energy* 182, 382–396, <https://doi.org/10.1016/j.solener.2019.02.054>.
- Zayed, M.E., Zhao, A.H., Elsheikh, F.A., Hammad, L., Ma, Y., Du, A., Kabeel, S.M., Shalaby, J., 2019b. Applications of cascaded phase change materials in solar water collector storage tanks: a review. *Sol. Energy Mater. Sol. Cells* 199, 24–49, <https://doi.org/10.1016/j.solmat.2019.04.018>.
- Zayed, M.E., Zhao, W., Li, A.H., Elsheikh, Z., Zhao, A., Khalil, J., Li, H., 2020. Performance prediction and techno-economic analysis of solar dish/stirling system for electricity generation. *Appl. Therm. Eng.* 164, 114427, <https://doi.org/10.1016/j.applthermaleng.2019.114427>.